DOI: 10.5604/01.3001.0054.3050

Volume 121 • Issue 2 • December 2023

Journal of Achievements in Materials and Manufacturing Engineering

International Scientific Journal published monthly by the World Academy of Materials and Manufacturing Engineering

Investigation of the impact of porosity of elements made using DMLS 3D printing technology and various printing angles on the mechanical properties and microstructure of 17-4 PH stainless steel

M. Deroszewska [a], R. Saraczyn [a,*], A. Cisowski [b], T. Kowaluk [c], T. Borowski [d], J. Petru [e], D. Myszka [a]

[a] Faculty of Mechanical and Industrial Engineering, Warsaw University of Technology, Pl. Politechniki 1, 00-665 Warszawa, Poland

[b] Faculty of Power and Aeronautical Engineering, Warsaw University of Technology, Pl. Politechniki 1, 00-665 Warszawa, Poland

[c] Faculty of Mechatronics, Warsaw University of Technology, Pl. Politechniki 1, 00-665 Warszawa, Poland

[d] Faculty of Materials Science and Engineering, Warsaw University of Technology, Pl. Politechniki 1, 00-665 Warszawa, Poland

[e] Faculty of Mechanical Engineering, Technical University of Ostrava, 708 00 Ostrava 8, Czech Republic

* Corresponding e-mail address: robert.saraczyn.dokt@pw.edu.pl

ORCID identifier: https://orcid.org/0000-0002-5195-8468 (R.S.)

ABSTRACT

Purpose: The research aimed to determine the impact of the degree of surface porosity of elements made using Direct Metal Laser Sintering (DMLS) 3D printing technology on the mechanical properties and structure of the elements by comparing the obtained test results with the standards and properties of elements manufactured using conventional methods.

Design/methodology/approach: 17-4 PH stainless steel was used to prepare the samples, from which two types of samples were printed. The elements were printed vertically and at an angle of 45° to the printer's working space. The assessment of material properties in a static tensile test was used to determine the state of stress and local strains using Digital Image Correlation. Additionally, hardness and surface roughness were measured. The structure of printed elements was also assessed using a light microscope, a scanning electron microscope and computer tomography with numerical porosity analysis.

Findings: The research showed a significant impact of porosity in concentrating and transferring stresses into the structure of the material, thus weakening the mechanical properties of the manufactured elements.

Research limitations/implications: The mechanisms of pore formation during 3D printing require in-depth analysis in various printer settings.

Practical implications: The mechanisms of pore formation in 3D printed metal materials affect the strength properties and, therefore, affect the applicability of the manufactured elements. Understanding the mechanisms will allow us to make corrections to technological processes.

Originality/value: The originality of the study lies in the link between the plastic behaviour of the material and the anisotropy of mechanical properties with the anisotropy of pore formation in elements 3D printed using DMLS technology.

Keywords: 3D printing, Direct metal laser sintering, 17-4 PH stainless steel, Porosity, Microstructure

Reference to this paper should be given in the following way:

M. Deroszewska, R. Saraczyn, A. Cisowski, T. Kowaluk, T. Borowski, J. Petru, D. Myszka, Investigation of the impact of porosity of elements made using DMLS 3D printing technology and various printing angles on the mechanical properties and microstructure of 17-4 PH stainless steel, Journal of Achievements in Materials and Manufacturing Engineering 121/2 (2023) 289-305. DOI: https://doi.org/10.5604/01.3001.0054.3050

1. Introduction

3D printing is an additive technology that is becoming increasingly popular and has a constantly growing range of applications. Currently, the technology is used to produce a wide range of industrial elements, starting from prototypes of parts of technical devices and machines in various industrial sectors (including automotive and aviation) through device components to full-scale products. The main advantages of 3D printing include the lack of need to use many specialised tools, flexibility in design, the ability to produce parts with lattice geometry and complex topology, mesh parts and their wide range of personalisation [1]. Using this technology, it is possible to produce products for various applications, including instruments and accessories, moulds of production tools, car parts, medical implants, aerospace parts, parts for sports applications and personalised elements [2]. 3D printing technology is supported by numerical modelling and computer simulations, which allow research and simulations to be carried out before printing, which allows for its initial assessment of physical phenomena occurring in a given element and thermomechanical behaviours that may occur during printing. The assessment can include the distribution of heat temperatures, the dynamics and geometry of the pool, phase transformations, melting and solidification, the quality of the microstructure, deformations and residual stresses [3]. Introducing the technology to the industry makes it much easier for manufacturers. Its use helps to eliminate design errors, shorten the time to introduce a new product to the market and reduce prototyping and production costs, which is crucial for unit and small-batch production [4].

To fully understand the processes occurring during additive manufacturing, it is also necessary to refer to the properties of steel produced using conventional methods. The tool and die industry requires using materials with high yield strength, hardness and abrasion resistance [5].

The research focuses on the relationship between the mechanical properties of the material and the structural discontinuities arising from the suboptimal 3D printing process. Table 1 describes the material from which the samples for testing were made – 17-4 PH.

Direct Metal Laser Sintering (DMLS) has many advantages over traditional metal fabrication methods. They include, among others, flexibility in creating geometry, consolidation of many parts, optimisation of material density, minimisation of post-production waste, and functionality. Such a technique also has limitations in metallurgical defects, i.e. folds, porosity, structure delamination, occurrence of high residual stresses, and surface roughness [6]. The appropriate selection of printing parameters significantly impacts the quality of manufactured elements. The combination of high temperature and high cooling rate, as well as heat treatment of the element, can significantly impact the microstructure and residual stresses [7].

Table 1.
Stainless Steel 17-4 PH Markforged – chemical content

Type	Name	Cr	Ni	Cu	Si	Mn	Nb	C	P	S	Fe
Stainless steel PH	17-4 PH	15-17.5%	3-5%	3-5%	1% max	1% max	0.15-0.45%	0.07% max	0.04% max	0.03% max	bal.

Solidification produces a very fine cellular microstructure, not a dendritic one, as in the case of castings. It virtually eliminates the dendritic segregation in conventional processing, eliminating the need for a chemical homogenisation step [8]. However, the structure is not without its drawbacks.

Particularly difficult to eliminate are post-process porosities resulting from incomplete melting of metal particles, released gases or impurities on the powder surface [9]. The quality of the structure and properties of the final element will also be influenced by the appropriate selection of printing process parameters [10,11]. The literature emphasises laser power, scan speed, overlap rate, layer thickness, hatching space, and building direction among the parameters that should be optimally selected. Suppose the delivered energy beam is insufficient to melt the powder. In such a case, much of it will remain in its initial state after production, resulting in voids in the element. A scanning speed that is too low may form a liquid phase on the particle surface, which will contribute to baking together the unmelted cores of particles into coarsened balls [11]. Research shows, for example, that there is a large dependence on parameters such as the hardness of the material or its resistance to brittle fracture depending on the laser power used during the 3D printing process [12]. The layer thickness may affect the impact strength value by insufficient distribution of the laser beam on the surface, leading to a lack of fusion and cracks in the places due to stress concentration [13]. Higher laser power in combination with lower scan speed can result in higher hardness due to a better energy transfer and high melting pool quality. Material hardness may decrease when hatch space values decrease below optimal due to a larger overlap.

On the other hand, for higher than optimal hatch spacing, due to the dispersion of beam energy, the hardness also tends to reduce its value [14]. When selecting process parameters, the metal powder and its geometric shape should also be taken into account to optimise the mechanical properties of the material. Depending on the technology in which the powder was made, its particles may vary in shape – from spherical, the most desirable, to elliptical, cylindrical or irregular shapes, the subsequent arrangement of which determines suboptimal welding [15].

2. Experimental

2.1. Research methodology

Research and analyses were conducted to determine the mechanical and structural properties of prints of 17-4 PH steel produced under variable arrangement angles of the printed layers. The printing technique used ensures light and durable parts.

The given research constitutes the basis for determining the properties of elements made with DMLS technology and, consequently, will contribute to the optimisation of their production process by assessing the impact of porosity on the structure of the entire element.

The test samples, described later in the article, were produced using 3D printing technology from powdered metal in DMLS technology based on a design created in SolidWorks software.

The work involved a static tensile test with digital image correlation, an impact test, material hardness measurement, surface roughness, microscopic tests and computed tomography tests.

2.2. Sample preparation and test procedure

3D printing of samples

The sample prints were made on an Orlas Coherent Creator printer, which has a working space in the shape of a cylinder, 100 mm high and 100 mm in diameter. The Fiber 250 laser ensures high beam quality and stability. The specified typical accuracy for such a type of device is 40µm. Table 2 shows the technical specifications of the Orlas Coherent Creator 3D printer. Hatch spacing used in the study was 40 µm, equal to the laser diameter due to 0% overlap. The laser power of 120W and a speed of 800 mm/s was used. The process parameters were selected to ensure the best possible quality of the raw print (without post-processing) – the lowest possible porosity, low surface roughness, and to limit residual stresses [16-19].

After printing, the supports were removed, and the manufactured elements were surface-treated and sandblasted.

Samples for static tensile testing and structure assessment using microscopic methods and computed tomography were printed using the sintering of successive layers in vertical and slanting positions (45° angle), as shown in Figure 1.

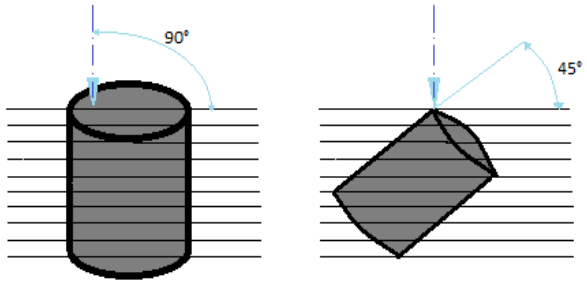

Fig. 1. The process of sintering subsequent layers in two positions: vertical and at an angle of 45°

Table 2.
Orlas Coherent Creator 3D printer – parameters used

Specification			
Laser type/power	Yb optical fiber laser/120 W	Spot size – laser diameter	40 µm
Wavelength	1070 nm	Shielding gas	nitrogen/argon
Working chamber	Φ100 mm x 100 mm	Cooling	Air
Powder distribution	Rotating, precise squeegee	Hatch spacing	40 µm
Layer thickness	25 µm	Laser speed	800 mm/s
Repeatability	X=15 µm, y=15 µm, z=15 µm	Boundary offset	80 µm
Min. workpiece size	X=80 µm, y=80 µm, z=20 µm	Material supply	Manual

Static tensile test and digital image correlation

Samples for the static tensile test were prepared according to the PN-EN ISO 6892-1:2010 standard shown in Figure 2 and arranged in the printer's working space by the visualisation shown in Figure 3. The static tensile test was performed on an Instron 8516 testing machine. Samples subjected to the static tensile test were also prepared using the digital image correlation method. First, a white spray layer was applied to the surface of the samples, and then the prepared surface was covered with randomly placed black dots. In this way, the samples were successively placed in the jaws of the testing machine and subjected to stretching. The test was performed at a speed of 0.1 mm/s.

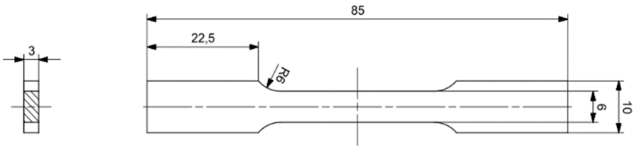

Fig. 2. Technical drawing of a sample prepared for a static tensile test

Impact test

The impact test was performed according to the PN-EN ISO 148-1:2010 standard. The first stage of sample preparation after determining their geometry was to create 3D models in SolidWorks in accordance with the specifications shown in Figure 4.

The sample is 55 mm long and has a square cross-section of 10 mm. In the middle of its length, there is a V-shaped notch with an angle of 45, a depth of 2 mm and a radius of rounding its bottom of 0.25 mm. The printouts are shown in Figure 5.

The samples were printed in two planes, shown in Figure 6. Twelve samples were made, including five printed in a vertical plane, which was selected to test the effect of material layering on impact strength. The remaining seven samples were in a slanting plane with an inclination angle of 45 degrees, shown in Figure 6, which was selected to achieve the highest notch accuracy during printing.

a)

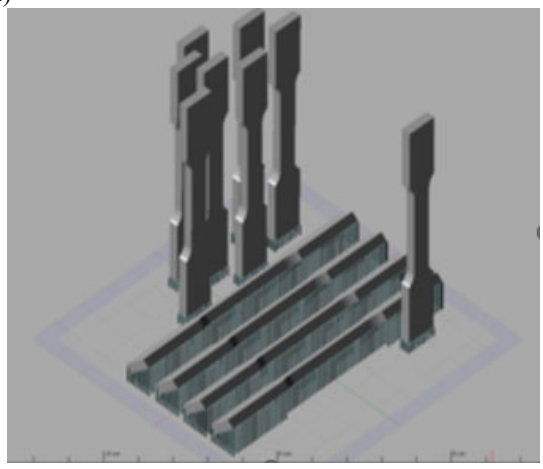

b)

Fig. 3. a) Visualisation of the arrangement of samples for static tensile testing during printing; b) Samples after 3D printing with DMLS technology prepared for static tensile testing

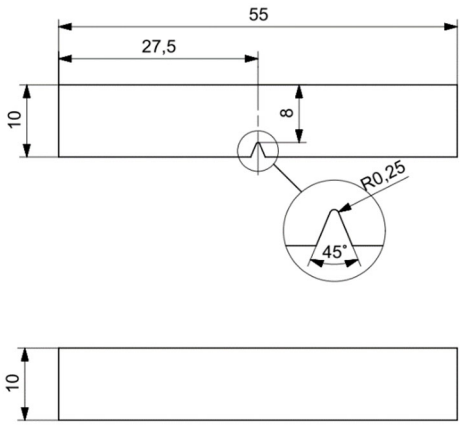

Fig. 4. Technical drawing of a sample for impact testing

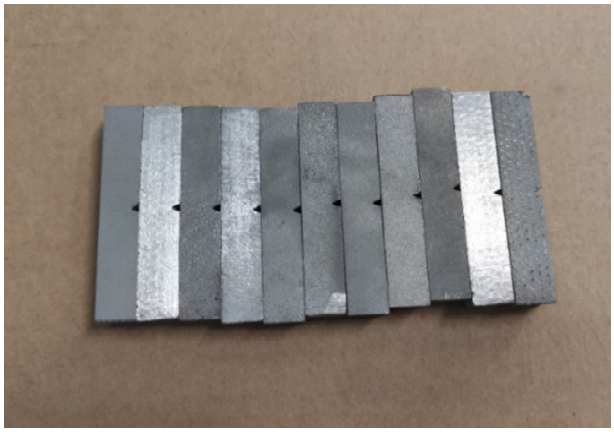

Fig. 5. Samples after 3D printing with DMLS technology prepared for impact testing

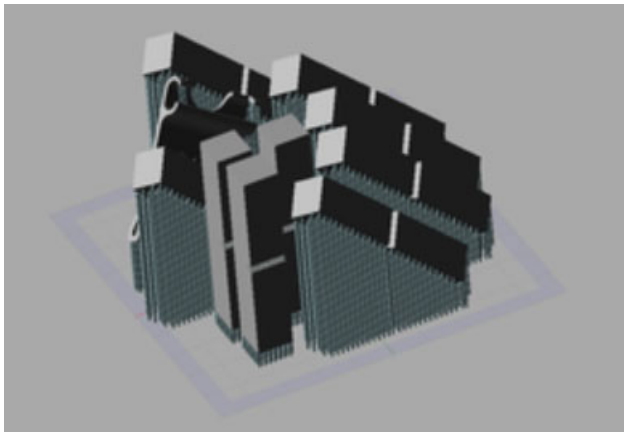

Fig. 6. Visualization of the arrangement of impact test samples during printing

A pendulum hammer, the so-called Charpy's hammer, was used for the test. The mounting of the samples in the jaws is illustrated in Figure 7.

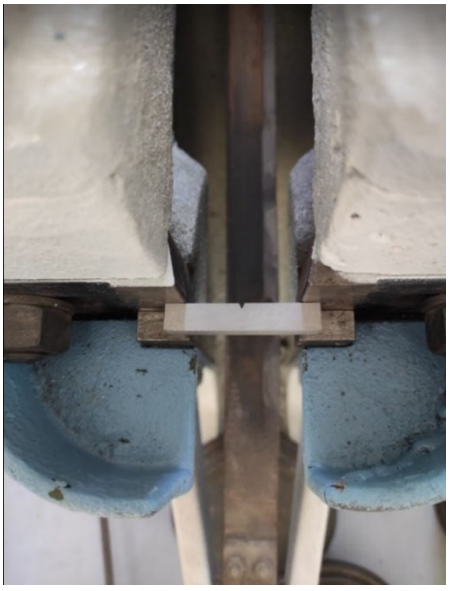

Fig. 7. View of mounting the sample for impact testing

During the test, the sample should lie perpendicularly on the supports so that the distance of the notch symmetry plane from the symmetry plane of the supports is not more than 0.5 mm. The sample should lie on supports in such a way that the blade of the pendulum knife hits the sample on the opposite side of the notch. If the test temperature is not specified in the relevant product standard, the test is carried out at 23°C +/- 5°C. It should be maintained within 2°C throughout the test.

Computed tomography and microscopic tests

Similar to the previously described research methods, in the case of structural tests, the first step in preparing samples was to design their geometry in the SolidWorks programme according to the specifications (Fig. 8).

Fig. 8. Technical drawing of a sample for microscopic examination in the form of a cylinder

The surface of two samples was subjected to microscopic examination, one printed in the arrangement shown in Figure 9 in a vertical plane, the other in a horizontal plane. Photos using a light microscope were taken at a resolution of 200 μm and with a magnification of x100.

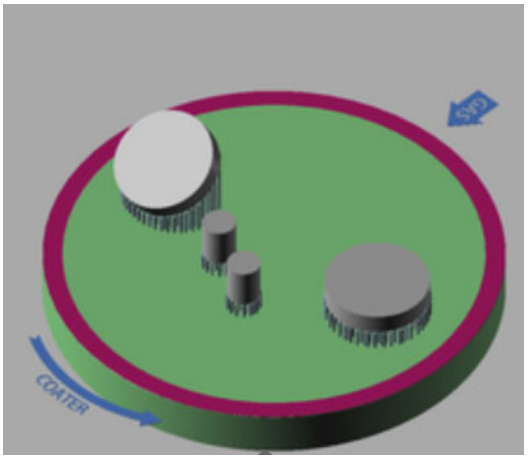

Fig. 9. Visualisation of the position of samples for microscopic examination and computed tomography during printing

The surface of the samples indicated in Figure 9 and Figure 10 was subjected to microscopic examination in two different configurations using a scanning electron microscope. First, the outer surface of the samples was examined, and then a cross-section of one of them was observed. The sample was prepared for observation through an inclusion process, which was intended to stabilise the sample in an inert material, in this case, a resin with the addition of graphite, to improve the conductivity of the material and, consequently, obtain a better quality image [20]. For such a purpose, a hot insertion press was first used, where the sample was placed in a resin matrix with an admixture of graphite. Heating took place at 200 °C and lasted about 7 minutes. Grinding and polishing the metal surface to a mirror shine was necessary. The following gradation weights of sandpaper were used: 80, 220, 400, 600, 800, 1000. At the final stage, the samples were etched from the microsection. The etching reagent, in such a case a mixture of hydrochloric acid and nitric acid, attacks primarily grain boundaries. The incident light is scattered thanks to the procedure, and the grain boundaries are observed in the microscope as dark lines.

First, properly prepared samples were placed in the microscope chamber. In the case of a scanning electron microscope, model S-3500N Hitachi, the surface microstructure imaging technique involves scanning the sample surface with a nanometre beam formed by the electro-optical system of the microscope. The beam is formed by a system of electromagnetic lenses and deflected using coils. The signal from the sample surface, in the form of secondary or backscattered electrons, reaches the detector, the most important parts of which are the scintillator and the photomultiplier.

a)

b)

Fig. 10. Samples for a) tomography, b) microscopic examination

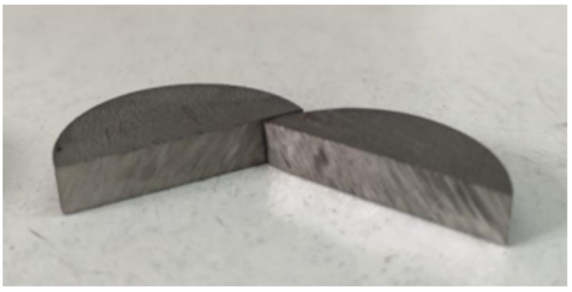

Fig. 11. Cross-section of a sample for microscopic examination

The scintillator converts the energies of secondary electrons into light pulses, which are then amplified by a photomultiplier. The signal from the detector controls the brightness of the image on the monitor. Images obtained during the tests were saved using a photographic method or digital recording. Then, the files were saved in the computer's memory. In the next stage, they were subjected to further analyses of the obtained image. Cross-sectional samples were also tested, as indicated in Figure 11.

The computed tomography examination was performed using Zeiss's Metrotom 800 computer X-ray tomograph. The device is used for dimensional inspection, detection of material defects and reverse engineering. It allows us to observe objects with complex geometry and hard-to-reach surfaces. CT examination parameters:

- X-ray tube with a voltage of 130 kV,
- measuring range: diameter 125 mm, height 150 mm,
- Maximum Permissible Error - $MPE_E = (4.5 + L/100)$ µm, where L is the measured length in mm,
- maximum mass of the tested object 4 kg,
- the time needed to scan an item fully is approximately two hours.

As a result of the tomographic measurement, a volume file is obtained with saved data in the form of voxels, each of which has the X, Y, and Z coordinate values and the grey scale value. The file is then loaded into data analysis software. The VGStudio MAX program was used in the tests, and in the programme, the data was processed, a porosity analysis was performed, and a series of cross-sections were generated, one in the TOP direction and one around the axis of rotation of the element.

Roughness measurement

The surface roughness measurement was carried out using a Mitutoyo contact roughness meter. The contact measurement involved determining the numerical parameters of the surface profile. The device allows direct reading of quantities such as the arithmetic mean deviation of the profile from the mean line – R_a, the height of roughness according to ten profile points – R_z, the mean square of the values inside the section – R_q. Samples for microscopic examination were used for the study – Figures 10b and 11.

Hardness test

The test was carried out using a Vickers HMV-G microhardness tester. It is an advanced hardness tester used to measure the hardness of metallic materials and ceramics. It enables the determination of the stress concentration coefficient. It is equipped with a Vickers indenter and Knoop, Brinell and triangular indenters, with two or four lenses.

In such a case, the Vickers hardness measurement was used. The principle of operation of the device is based on indenting a four-sided regular diamond pyramid with a vertex angle of 136° into the surface of the tested material under a given static load (1 kg) and then measuring the diagonals of the resulting square impression. The numerical value of hardness is obtained by the ratio of the load to the lateral surface area of the pressure. Samples for microscopic examination were used for the study – Figures 10b and 11.

3. Results and discussion

The test results were analysed with particular emphasis on understanding the influence of the surface structure of the samples on the stress distribution and strength properties of the printed elements. There was a correlation of the results of destructive tests, i.e. static tensile test and Charpy impact test, with non-destructive tests, i.e. electron microscopy, computed tomography and surface roughness testing. An important issue in the context of the mechanism of defect formation on the surface of printed elements is the orientation of the print and related phenomena causing different distributions of voids in the printed element. The results of the static tensile test are presented in Table 3 and Figures 12 and 13.

Table 3.
Results of tensile strength test for Vertical 1-3 and Slanting 1-3 samples

	Stress at failure, MPa	Strain at failure, %	Maximum stress, MPa
Vertical 1	486.18	19.49	703.47
Vertical 2	511.72	18.34	706.61
Vertical 3	465.87	16.98	727.56
Slanting 1	701.73	9.57	825.06
Slanting 2	707.99	16.19	856.57
Slanting 3	740.09	13.42	842.53

The average maximum stress value was 712.55 ±12.097 (±1.7%) MPa for the Vertical category and 841.39 ±14.586 (±1.7%) for the Slanting category.

The results indicate that samples printed at a 45-degree angle to the printer's build surface exhibit higher tensile strength by approximately 15%. A clear yield point can be observed for both orientations, which occurs at approximately 2% of the sample deformation. Samples printed at an angle are also characterised by smaller deformation than samples printed vertically – by an average of 40%. It indicates a very different behaviour of the material

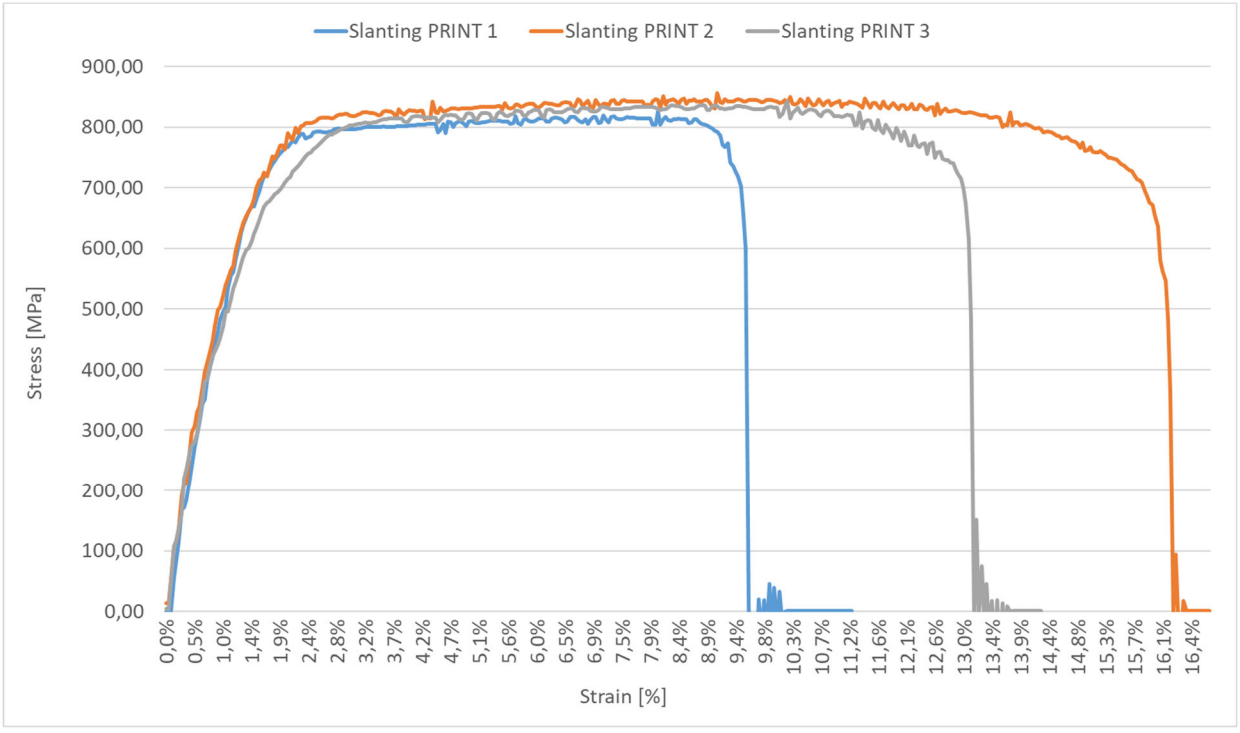

Fig. 12. Stress – Strain diagram for slanting samples

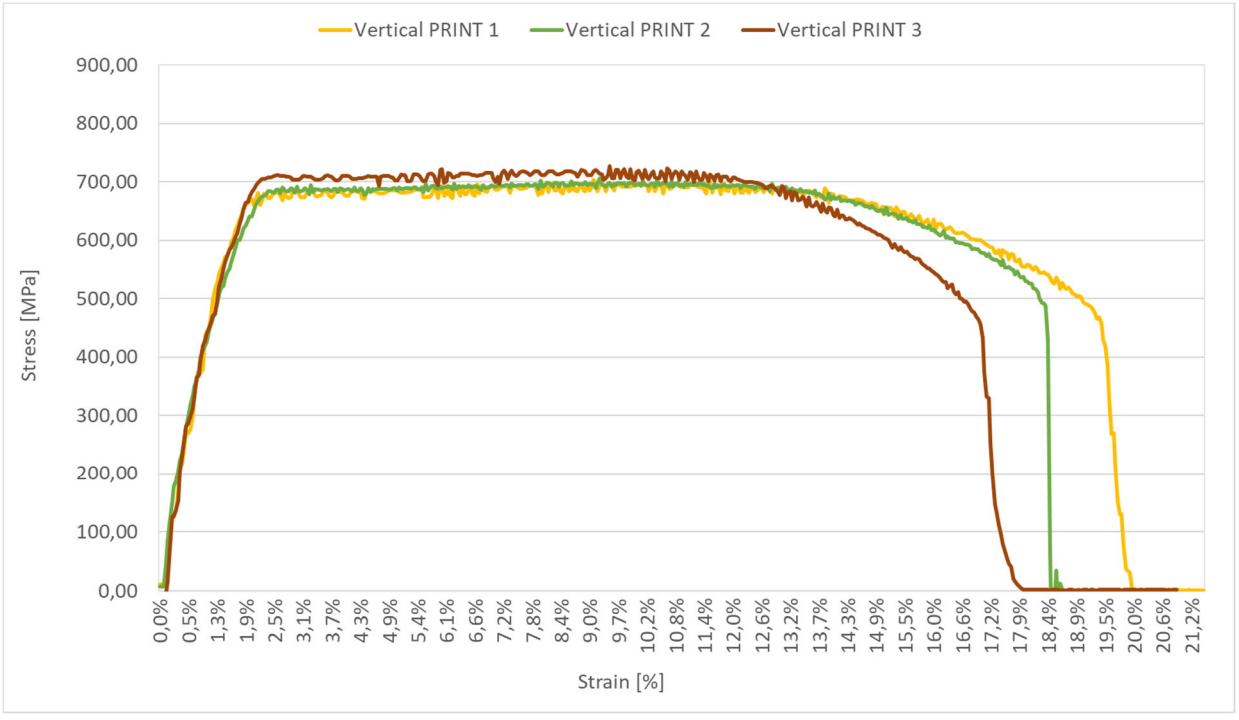

Fig. 13. Stress – Strain diagram for vertical samples

and suggests that the porosity volume may significantly impact the elasticity of the material under load. Undoubtedly, the volume of pores influences the difference in the strength of the material [21,22]. Still, such a significant difference in deformation should not be associated solely with the location, density or volume of porosity. The ductility is expected to be lower due to the acceleration of the crack propagation process within the voids [23,24]. However, we observe the opposite behaviour here, which is intuitively not directly related to the volume of voids or their spatial distribution but to the printing angle [25,26]. For both samples, the cracking mechanism was a bit different and depended on the position of the sample in the machine relative to its printing plane. Vertical samples were torn off along the printing plane while slanting crosswise, as shown in Figure 3a. We do not observe significant differences in elongation in the case of samples printed vertically.

In contrast, for samples printed at an angle of 45 degrees, the differences in deformability within the group are exceptionally large. Therefore, it is not related to the direction of printing itself but to the anisotropy of the pores in relation to the direction of the applied load, which may cause anisotropy of mechanical properties [27]. Interlayer pores lead to the formation of residual stresses, which consequently reduce the plasticity of the material [28]. More stochastic pore formation would be expected when printing at a 45-degree angle due to possible shifting of the sintered powder granules. It may be the reason for differences in elongation within one group of samples printed at the same angle. The difference in elongation between samples printed at an angle and those printed vertically may also be related to the mechanics of pore formation and their subsequent impact on the propagation of stresses inside the material.

The obtained tensile strength values should be compared with the material's datasheet, where the manufacturer predicts Rm at 800 MPa and Re at 1050 MPa. The strength results obtained are lower than those declared by the manufacturer but higher than those of analogous tests for SLM 3D printing technology [22].

During the static tensile test, the camera system analysed points on the surface of the samples, making it possible to assess the stress distribution [29,30]. In the case of a sample printed vertically, an accumulation of stresses can be observed in a narrow cross-section of the sample. In contrast, in the case of a sample printed at an angle, the stresses are distributed throughout practically the entire measuring part. The accumulation of stresses in the bottleneck may indicate defects that caused the sample to break under a lower load. Defects should be looked for where the material was torn off. Figures 14 and 15 indicate that vertically printed samples have more ductile fracture, while slanting samples have more brittle fracture.

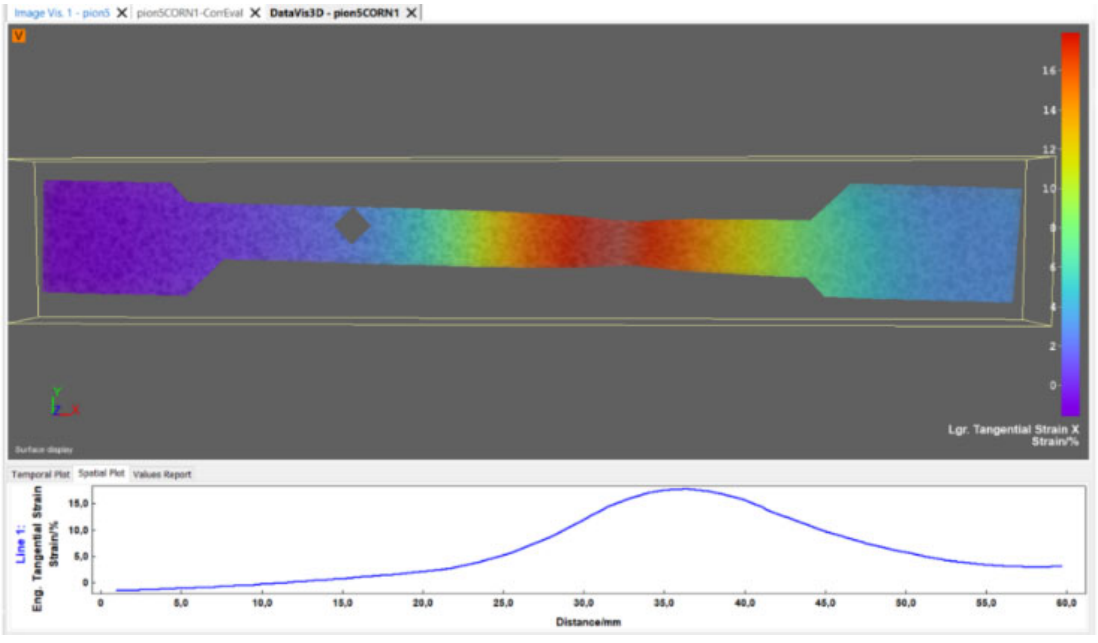

Fig. 14. Values of sample deformation as a function of displacement - sample no. 2 printed in a vertical plane, just before breaking

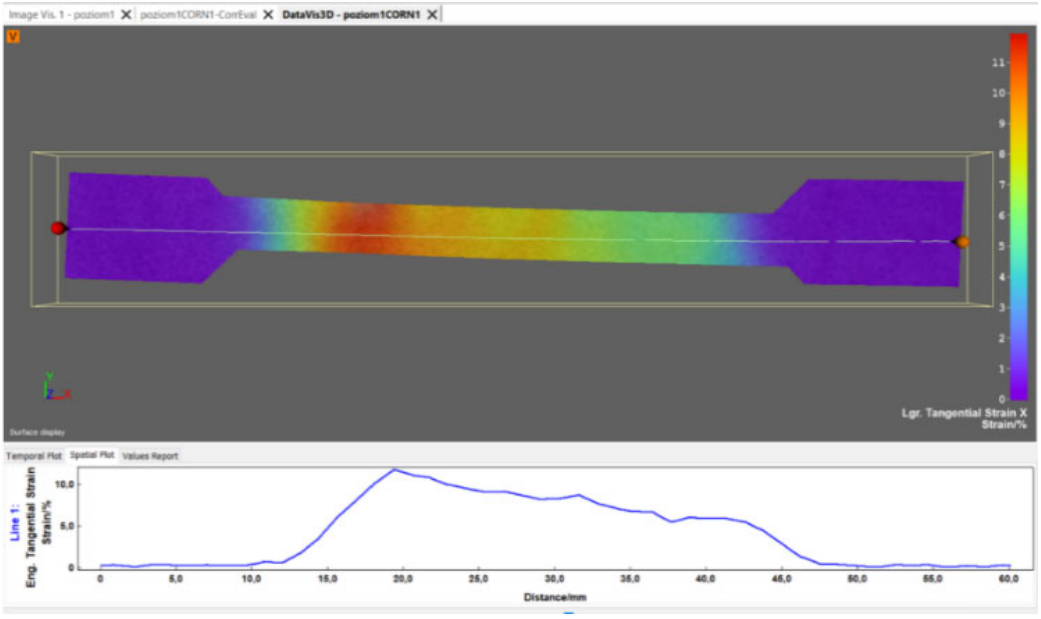

Fig. 15. Values of sample deformation as a function of displacement – sample no. 2 printed in a plane at an angle of 45 degrees, just before breaking

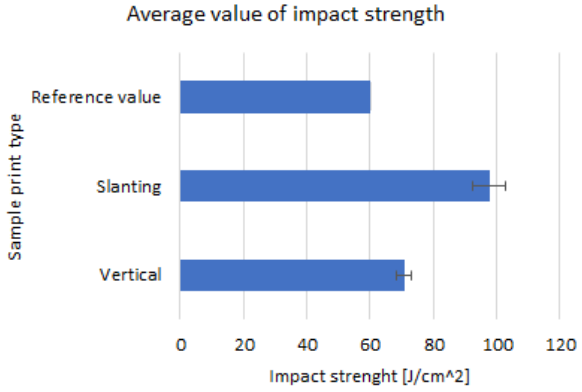

Fig. 16. Impact test results for DMLS samples – vertical and slanting

Figure 16 shows the average impact strength value depending on the printing angle. The reference value is the minimum crack resistance in the transverse direction under dynamic load for stainless steel, acc. PN-EN 10088-2:2014 standards. The average result obtained for samples printed at an angle is much higher than for those printed vertically, i.e. by approximately 43%. The impact strength value obtained for the slanting orientation was 97.88 ±5.092 (±5.2%), and for the vertical orientation, it was 70.77 ±2.399 (±3.3%). The standard deviation was 5.38 for the slanting orientation and 5.57 for the vertical orientation. The reason for such a large difference in the impact strength values of the materials should be sought in the microstructure of the samples, with particular emphasis on the continuity and composition of the material microstructure, the occurring material inclusions and the porosity of the structure.

Analysis of the porosity structure of samples throughout their cross-section is possible thanks to computed tomography [31,32], as shown in Figures 17-20. The volumetric voids can be defined by analysing Figures 18 and 19. Figure 19b, compared to Figure 19a, shows that the structure discontinuities in vertically printed samples are more dispersed in the sample space. Discontinuities in samples printed at an angle are limited to the central part of the sample and are characterised by smaller volumes. To estimate the porosity of the structure, a computer programme for image analysis was prepared, which counted the number of pores (understood as one pixel equals one pore). For Figure 18a, this value was 659 pores; for Figure 18b, it was 466 pores; for Figure 19a, it was 185 pores; for Figure 19b, it was 156 pores. The analysis of the porosity distribution (using CT software) inside the entire sample showed that the total pore volume in relation to the sample volume for slanting printed samples was 2.34%. In comparison, for vertically printed samples, it was 2.50%. The porosity distribution also indicates that vertically printed samples are characterised by larger (in volume) individual pores, which contribute to the propagation of stresses inside the material to a greater extent than a few smaller voids.

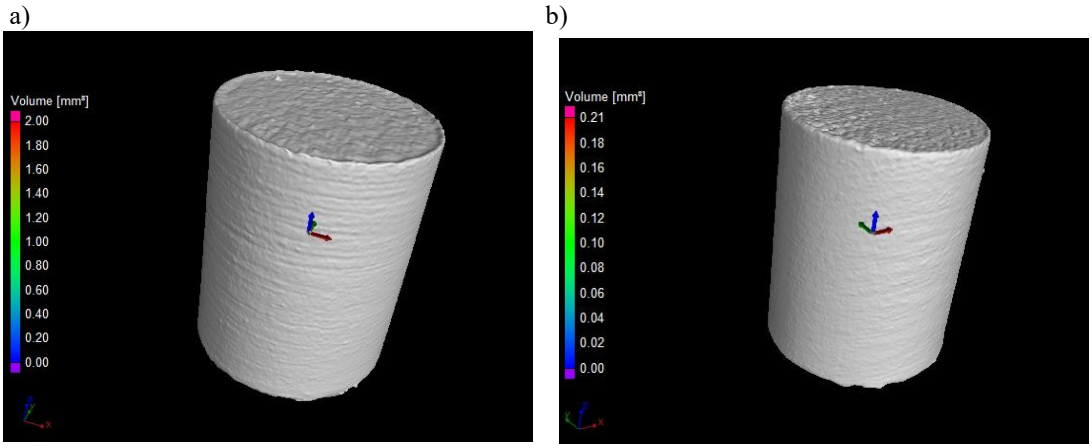

Fig. 17. Lateral plane, side view: a) vertical print, b) slanting print

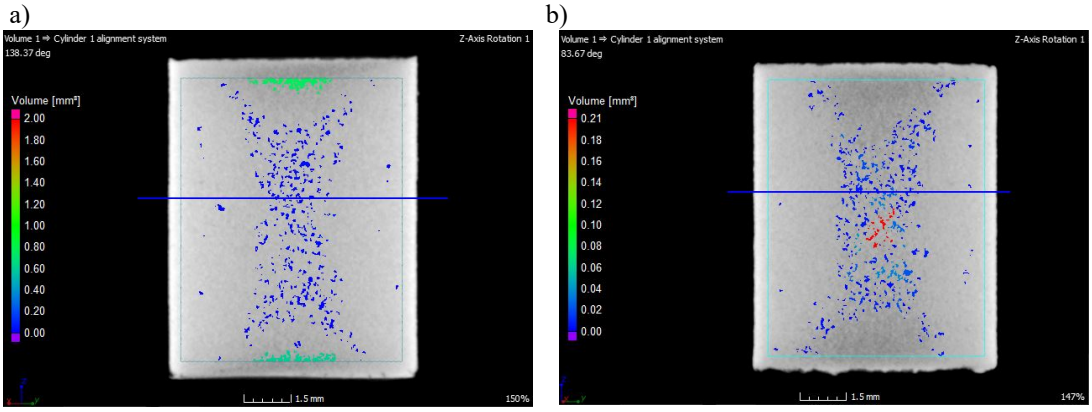

Fig. 18. Lateral plane: a: vertical print, b) slanting print

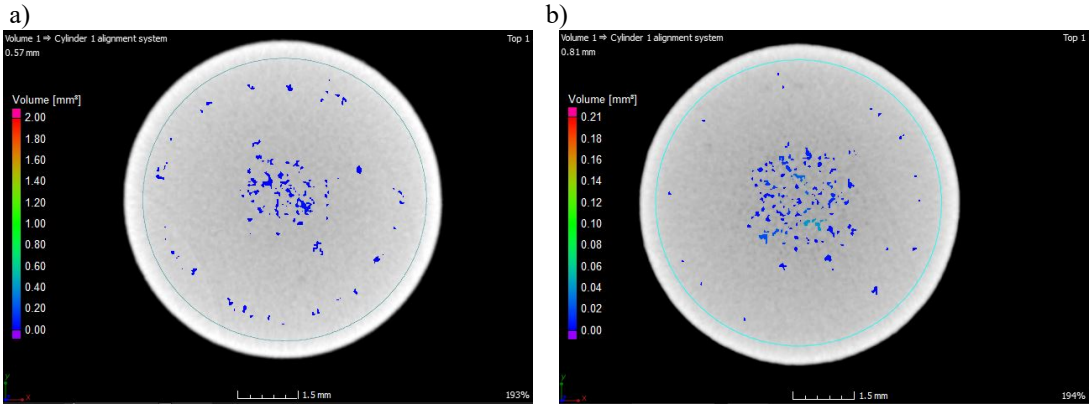

Fig. 19. Upper plane: a) vertical print, b) slanting print

Interestingly, in both cases, the largest accumulation of structural discontinuities occurs in the areas furthest from the edge of the sample, as illustrated in Figure 18a and Figure 18b. This may be due to insufficient melting of the substrate and partially melted powders near the border of the molten metal pool [33]. Still, it may also result from

insufficient laser energy, which results in incomplete melting of metal powders, which in turn involves the binding of only partially melted powders [34]. It is also possible for gas to be captured by molten metal during the crystallisation process [35].

Figure 20a shows a band of material porosity with a large total volume in the case of a vertically printed sample. In a similar place of the sample printed at an angle of 45 degrees, Figure 20b, such compaction does not occur, although it is visible that porosity is locally present. It is correlated with observations made on Figures 18a and 18b which show that in the upper and lower parts of the sample, at approximately the same distance from the edge of the sample, porosity bands are formed (marked with green line), where this porosity is the largest in volume in the entire sample – approximately 5 times greater than other voids in the material (1 mm^2).

CT provides high quality image analysis among the techniques used, which allows to indicate the volume of porosity with an accuracy of hundredths of a mm [36].

Figure 21 shows the largest surface defects for samples tested using light microscopy. Surface defects are clearly visible in the case of elements printed in a vertical plane. Figure 21a illustrates discontinuities and delaminations, the origin of which should be attributed to insufficient fusion or low laser penetration depth [37].

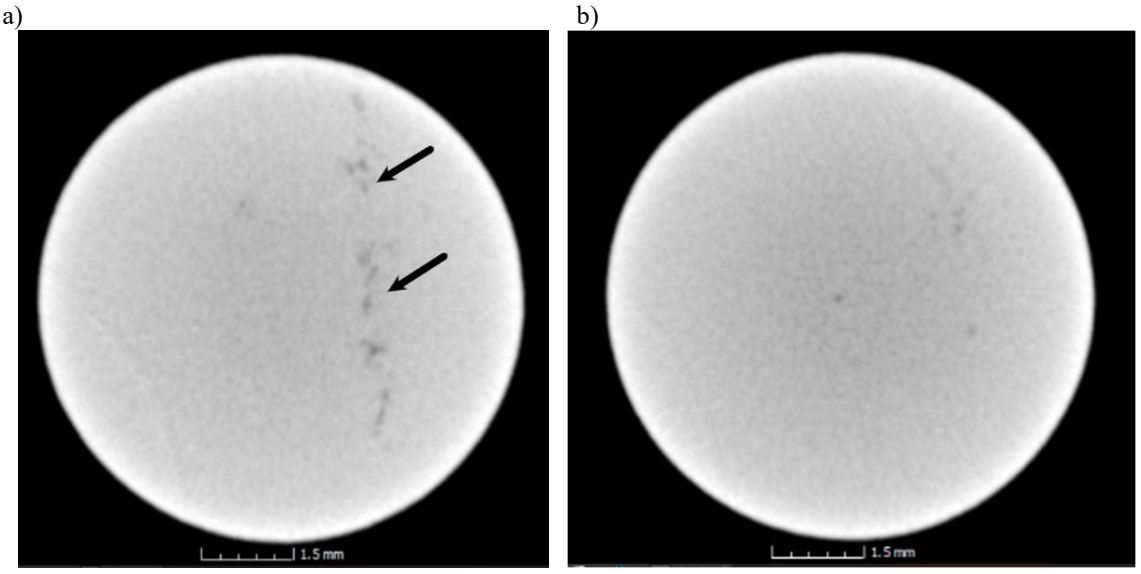

Fig. 20. a) Vertical print – upper plane, porosity belt, b) slanting print – upper plane, corresponding view

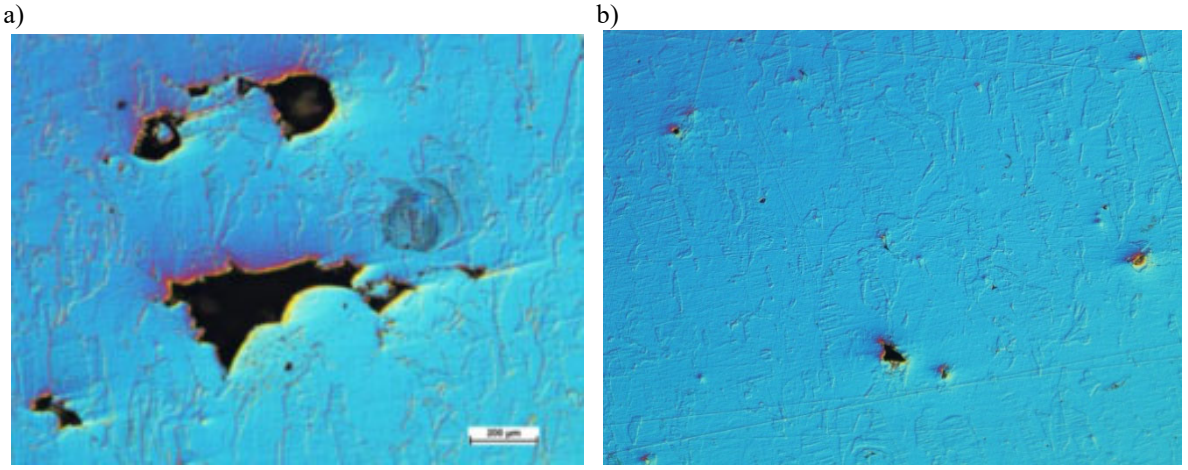

Fig. 21. Sample no. 2: a) printed in a vertical plane, b) printed in a slanting plane

Figures 22 and 23 show the structure of the middle surface of the sample for microscopic examination with 250x and 1000x magnification, respectively. The surface varies in size and distribution of structural defects. Because the strength of a sample is determined by its largest defects [27, 38-40], it should be assumed that there is a correlation between the achieved tensile strength values and the surface structure of the analysed samples [41].

The surface roughness was measured, where the parameters R_z (roughness height according to ten points of the profile), R_q (average amplitude deviation of the profile from the average line along the measurement section) and R_a (average arithmetic deviation of the profile from the average line) were determined, as illustrated in Figure 24. The average R_z value for the slanting plane was 73.24 ±2.241 (±3.1%), while for the vertical plane, it was 59.18 ±1.629 (±2.7%). The average R_q value for the slanting plane was 14.70 ±0.577 (±3.9%), while for the vertical plane was 11.93 ±0.475 (±4.0%). The average R_a value for the slanting plane was 11.47 ±0.407 (±3.6%), while for the vertical plane was 9.47 ±0.328 (±3.5%). The results obtained induce relatively high surface roughness, considering 3D printing technology [42,43]. However, it should be noted that in accordance with the PN-EN ISO 1302:2004 standard, samples made using DMLS technology correspond to the roughness obtained in milling or rolling processes and, in the case of vertical print orientation, even injection casting.

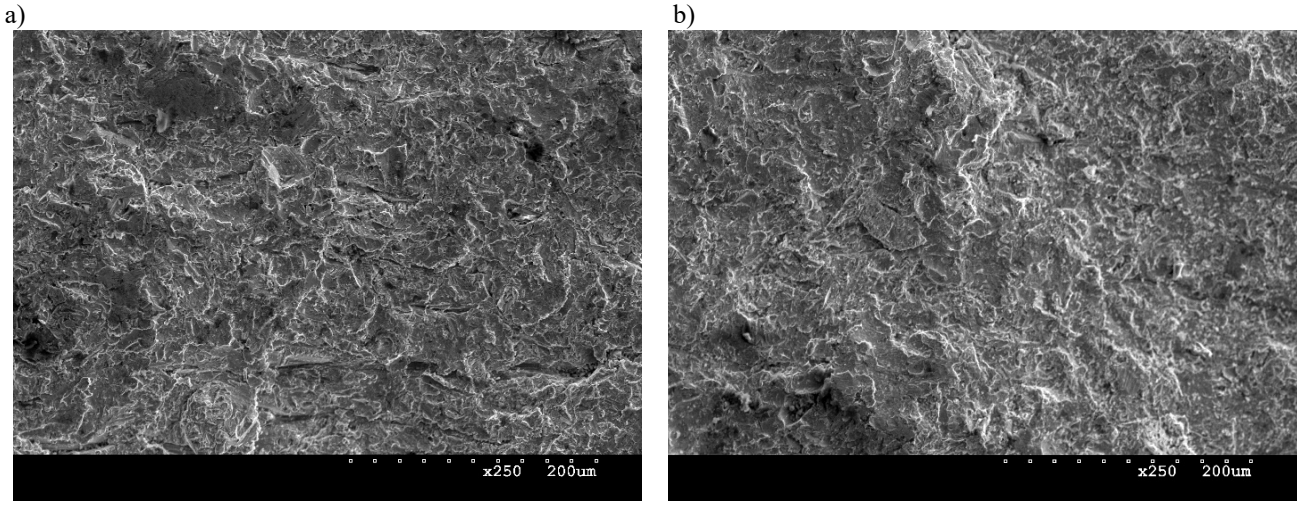

Fig. 22. a) vertical print, b) slanting print, magnification x250

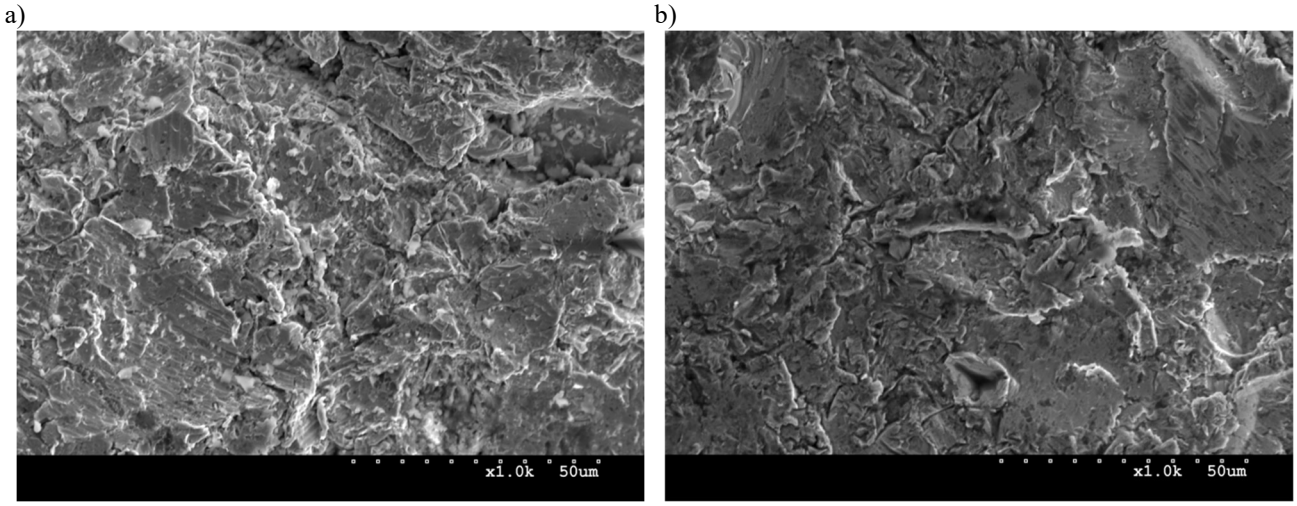

Fig. 23. a) vertical print, b) slanting print, magnification x1000

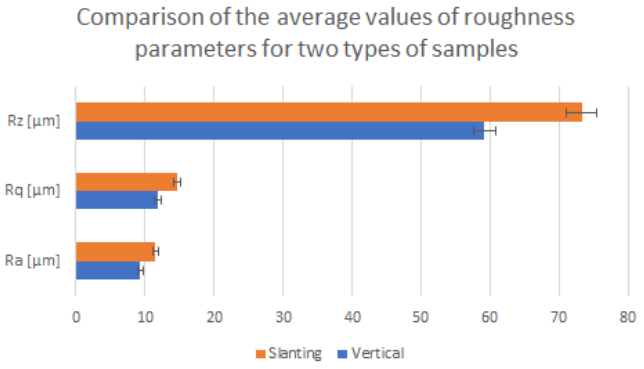

Fig. 24. Comparison of the average values of roughness parameters for two types of samples

Finally, the hardness was measured and, as before, compared to the reference value resulting from the PN-EN 10088-1:2014-12 standard. It should be noted, however, that the manufacturer of the metal powder used in the study predicted a hardness of 30 HRC on the Rockwell scale, corresponding to 285 HV on the Vickers scale. Therefore, in relation to the hardness expected based on the datasheet, samples printed at an angle reach almost the specification sheet value – 283.6 ±5.092 (±1.8%) HV – while samples printed vertically have a much lower hardness level, i.e. 274 ±4.753 (±1.7%) HV, as shown in Figure 25. The relationship should be sought in the density of the material, i.e. the ratio of the volume of porosity present in the structure to the theoretically solid structure [44]. In such a case, samples printed using DMLS 3D printing technology show a lower hardness value for material than the minimum specified in the standards.

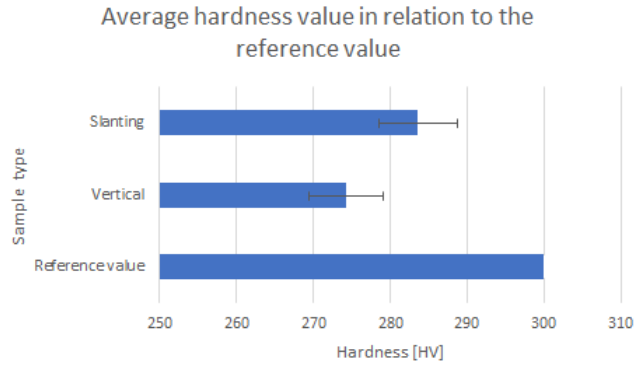

Fig. 25. Comparison of the average values of hardness parameters for two types of samples

4. Conclusions

The study showed that elements printed from 17-4 PH steel using DMLS 3D printing technology could be successfully used as construction materials for elements with complex geometry, where the cost of producing individual elements using conventional methods would be disproportionately high. This is due to the relatively high strength, ductility, and hardness of samples made using the method compared to classical technologies and the quite good surface quality. However, surface treatment of printed parts is advisable, as indicated by the high surface roughness – R_z of 73.24 ±2.241 (±3.1%) µm for samples printed at an angle and 59.18 ±1.629 (±2.7%) µm for samples printed vertically.

Printing from 17-4 PH steel using DMLS technology is characterised by a significant amount of porosity in the structure, which affects the mechanical properties of the manufactured elements. However, it should be noted that the porosity of the samples depends on the process parameters, and appropriate manipulation of them allows for the reduction of the porosity. Process parameters should be selected appropriately each time, considering the geometry to be printed and the material used in the manufacturing process.

In the case of samples printed vertically, the accumulation of stresses was concentrated in a narrow cross-section of the sample, associated with the accumulation of large-volume porosities. In contrast, the stresses were distributed throughout the measuring part in samples printed. The porosity dispersion analysis indicated by CT coincided with the stress concentration indicated by DIC.

The influence of the porosity volume on the elastic behaviour of the material under load was noticed. The phenomenon is related to the observed yield strength, which for samples printed in the slanting orientation is lower than the reference value from the material safety data sheet by 17% and for samples in the vertical orientation by as much as 37%.

Pores in the case of angled printing are characterised by a more stochastic formation mechanism due to the irregular shifting of metal powder particles due to the influence of gravity and the laser beam. It should be related to the results of the strength tests that indicate that samples printed at a 45-degree angle to the printer's build surface exhibit higher tensile strength by approximately 15%.

Differences in deformability within the group of samples printed at an angle of 45 degrees are relatively large, which should be associated with the anisotropy of the pores formed in relation to the direction of the applied load. Thus, the anisotropy of strength properties through different

mechanics of crack propagation inside the material weakens the entire structure.

Research funding

The research received no external funding.

Contributions

Conceptualization: R.S., M.D., D.M., methodology, M.D., D.M., R.S., project administration M.D., R.S., D.M., processing of results R.S., M.D., software R.S., M.D., D.M., J.P., supervision D.M., validation M.D., D.M., R.S., material preparation M.D., R.S., A.C., J.P., tensile tests A.C., computed tomography T.K., scanning electron microscopy T.B. All authors read and agreed to the published version of the manuscript.

Conflict of interest

The authors declare no conflict of interest.

Consent for publication

All the authors are pleased to publish the manuscript in the Journal of Achievements in Materials and Manufacturing Engineering.

References

[1] P. Ninpetcha, P. Kowitwarangkul, S. Mahathanabodee, P. Chalermkarnnon, P. Ratanadecho, A review of computer simulations of metal 3D printing, AIP Conference Proceedings 2279 (2020) 050002. DOI: https://doi.org/10.1063/5.0022974

[2] V. Bhavar, P. Kattire, V. Patil, S. Khot, K. Gujar, R. Singh, A Review on Powder Bed Fusion Technology of Metal Additive Manufacturing, Proceedings of the International Conference and Exhibition on Additive Manufacturing Technologies "AM-2014", Banglore, India, 2014.

[3] M. Markl, C. Korner, Multi-Scale Modeling of Powder-Bed-Based Additive Manufacturing; Annual Review of Materials Research 46 (2016) 93-123. DOI: https://doi.org/10.1146/annurev-matsci-070115-032158

[4] M. Meng, J. Wang, H. Huang, X. Liu, J. Zhang, Z. Li, 3D printing metal implants in orthopedic surgery: Methods, applications and future prospects; Journal of Orthopaedic Translation 42/1 (2023) 94-112. DOI: https://doi.org/10.1016/j.jot.2023.08.004

[5] P. Bajaj, A. Hariharan, A. Kini, P. Kürnsteiner, D. Raabe, E.A. Jägle, Steels in additive manufacturing: A review of their microstructure and properties, Materials Science and Engineering: A 772 (2020) 138633. DOI: https://doi.org/10.1016/j.msea.2019.138633

[6] P. Humnabad, R. Tarun, I. Das, An Overview of Direct Metal Laser Sintering (DMLS) Technology for metal 3D Printing, Journal of Mines Metals and Fuels 70/3A (2022) 127-133. DOI: https://doi.org/10.18311/jmmf/2022/30681

[7] M. Anand, A.K. Das, Issues in fabrication of 3D components through DMLS Technique: A review, Optics and Laser Technology 139 (2021) 106914. DOI: https://doi.org/10.1016/j.optlastec.2021.106914

[8] S. Yamashita, R. Yamauchi, K. Saida, Influence Mechanism of Solidification Mode on Solidification Cracking Susceptibility of Stainless Steels; Japan Welding Society 40/2 (2022) 67-76 (in Japanese). DOI: https://doi.org/10.2207/qjjws.40.67

[9] H.-H. Lai, H. Hsieh, C.-Y. Kuo, W. Wu, Solidification cracking nature and sequence of different stainless steels, Journal of Materials Research and Technology 25 (2023) 1030-1040. DOI: https://doi.org/10.1016/j.jmrt.2023.06.017

[10] C.-C. Kuo, X.-Y. Yang; Optimization of direct metal printing process parameters for plastic injection mold with both gas permeability and mechanical properties using design of experiments approach; The International Journal of Advanced Manufacturing Technology 109 (2020) 1219-1235. DOI: https://doi.org/10.1007/s00170-020-05724-w

[11] P. Hanzl, M. Zetek, T. Baksa, T. Kroupa, The Influence of Processing Parameters on the Mechanical Properties of SLM Parts, Procedia Engineering 100 (2015) 1405-1413. DOI: https://doi.org/10.1016/j.proeng.2015.01.510

[12] A.A. Deev, P.A. Kuznetcov, S.N. Petrov, Anisotropy of mechanical properties and its correlation with the structure of the stainless steel 316L produced by the SLM method, Physics Procedia 83 (2016) 789-796. DOI: https://doi.org/10.1016/j.phpro.2016.08.081

[13] V.S. Sufiiarov, A.A. Popovich, E.V. Borisov, I.A. Polozov, D.V. Masaylo, A.V. Orlov, The effect of layer thickness at selective laser melting, Procedia Engineering 174 (2017) 126-134. DOI: https://doi.org/10.1016/j.proeng.2017.01.179

[14] A.M. Khorasani, I. Gibson, U.S. Awan, A. Ghaderi, The effect of SLM process parameters on density, hardness, tensile strength and surface quality of Ti-6Al-4V, Additive Manufacturing 25 (2019) 176-186. DOI: https://doi.org/10.1016/j.addma.2018.09.002
[15] R. Baitimerov, P. Lykov, D. Zherebtsov, L. Radionova, A. Shultc, K.G. Prashanth, Influence of Powder Characteristics on Processability of AlSi12 Alloy Fabricated by Selective Laser Melting, Materials 11/5 (2018) 742. DOI: https://doi.org/10.3390/ma11050742
[16] S.A. Fatemi, J. Z. Ashany, A.J. Aghchai, A. Abolghasemi, Experimental investigation of process parameters on layer thickness and density in direct metal laser sintering: a response surface methodology approach, Virtual and Physical Prototyping 12/2 (2017) 133-140. DOI: https://doi.org/10.1080/17452759.2017.1293274
[17] J. Delgado, J. Ciurana, C.A. Rodriguez, Influence of process parameters on part quality and mechanical properties for DMLS and SLM with iron-based materials, The International Journal of Advanced Manufacturing Technology 60 (2012) 601-610. DOI: https://doi.org/10.1007/s00170-011-3643-5
[18] M. Król, J. Mazurkiewicz, S. Żołnierczyk, Optimization and analysis of porosity and roughness in selective laser melting 316L parts, Archives of Materials Science and Engineering 90/1 (2018) 5-15. DOI: https://doi.org/10.5604/01.3001.0012.0607
[19] P.K. Nayak, A.K. Sahu, S.S. Mahapatra, Effect of Process Parameters on the Mechanical Behavior of FDM and DMLS Build Parts, Materials Today: Proceedings 22/4 (2020) 1443-1451. DOI: https://doi.org/10.1016/j.matpr.2020.01.502
[20] G. Mrówka-Nowotnik, The effect of intermetallics on the fracture mechanism in AlSi1MgMn alloy, Journal of Achievements in Materials and Manufacturing Engineering 30/1 (2008) 35-42.
[21] W. Zhang, L. Li, J. Gao, J. Huang, X. Zhang, The Effect of Porosity on Mechanical Properties of Porous FeCrN Stainless Steel, Journal of Physics: Conference Series 2044 (2021) 012002. DOI: https://doi.org/10.1088/1742-6596/2044/1/012002
[22] S. Kedziora, T. Decker, E. Museyibov, J. Morbach, S. Hohmann, A. Huwer, M. Wahl, Strength Properties of 316L and 17-4 PH Stainless Steel Produced with Additive Manufacturing, National Library of Medicine Materials 15/18 (2022) 6278. DOI: https://doi.org/10.3390/ma15186278
[23] R. Reiff-Musgrove, W. Gu, J. E. Campbell, J. Reidy, A. Bose, A. Chitrapur, Y. Tang, M. Burley, T. Clyne, Effect of Relatively Low Levels of Porosity on the Plasticity of Metals and Implications for Profilometry-Based Indentation Plastometry, Advanced Engineering Materials 24/12 (2022) 202200642. DOI: https://doi.org/10.1002/adem.202200642
[24] R. Saraczyn, M. Deroszewska, T. Kowaluk, E. Skołek, W. Rządkowski, D. Myszka, Supported by 2D and 3D Imaging Methods Investigation of the Influence of Fiber Orientation on the Mechanical Properties of the Composites Reinforced with Fibers in a Polymer Matrix, Advances in Science and Technology Research Journal 17/3 (2023) 170-183. DOI: https://doi.org/10.12913/22998624/166101
[25] T. Alkindi, M. Alyammahi, R. A, Susantyoko, S. Atatreh, The effect of varying specimens printing angles to the bed surface on the tensile strength of 3D-printed 17-4PH stainless-steels via metal FFF additive manufacturing, MRS Communications 11 (2021) 310-316. DOI: https://doi.org/10.1557/s43579-021-00040-0
[26] M.M. Hanon, Y. Alshammas, L. Zsidai, Effect of print orientation and bronze existence on tribological and mechanical properties of 3D-printed bronze/PLA composite, May 2020, The International Journal of Advanced Manufacturing Technology 108 (2020) 553-570. DOI: https://doi.org/10.1007/s00170-020-05391-x
[27] A.D. Baghi, S. Nafisi, R. Hashemi, H. Ebendorff-Heidepriem, R. Ghomashchi, Experimental realisation of build orientation effects on the mechanical properties of truly as-built Ti-6Al-4V SLM parts, Journal of Manufacturing Processes 64 (2021) 140-152. DOI: https://doi.org/10.1016/j.jmapro.2021.01.027
[28] M.G. Moletsane, P. Krakhmalev, N. Kazantseva, A. du Plessis, I. Yadroitsava, I. Yadroitsev, Tensile properties and microstructure of direct metal laser-sintered Ti6Al4V (ELI) alloy, South African Journal of Industrial Engineering 27/3 (2016) 110-121. DOI: https://doi.org/10.7166/27-3-1667
[29] B. Demchyna, M. Surmai, R. Tkach, The experimental study of glass multilayer columns using digital image correlation, Archives of Materials Science and Engineering 96/1 (2019) 32-41. DOI: https://doi.org/10.5604/01.3001.0013.1990
[30] G. Kokot, K. Skalski, A. Makuch, W. Ogierman, Digital image correlation and nanoindentation in evaluation of material parameters of cancellous bone microstructure, Archives of Materials Science and Engineering 83/1 (2017) 10-16. DOI: https://doi.org/10.5604/01.3001.0009.7536
[31] H. Dinnebier, I. Ehrlich, The effects of severe temperature changes and high humidity on porous CFRP, Journal of Achievements in Materials and Manufacturing Engineering 67/1 (2014) 14-20.
[32] P. Malara, L.B. Dobrzański, Computer-aided design and manufacturing of dental surgical guides based on

cone beam computed tomography, Archives of Materials Science and Engineering 76/2 (2015) 140-149.
[33] S. Wang, J. Ning, L. Zhu, Z. Yang, W. Yan, Y. Dun, P. Xue, P. Xu, S. Bose, A. Bandyopadhyay, Role of porosity defects in metal 3D printing: Formation mechanisms, impacts on properties and mitigation strategies, Materials Today 59 (2022) 133-160. DOI: https://doi.org/10.1016/j.mattod.2022.08.014
[34] Z. Wang, Ch. Wang, Ch. Li, Y. Qin, L. Zhong, B. Chen, Z. Li, H. Liu, F. Chang, J. Wang, Analysis of factors influencing bone ingrowth into three-dimensional printed porous metal scaffolds: A review, Journal of Alloys and Compounds 717 (2017) 271-285. DOI: https://doi.org/10.1016/j.jallcom.2017.05.079
[35] S.V. Adjamskyi, G.A. Kononenko, R.V. Podolskyi, Influence of technological parameters of slm-process on porosity of metal products, The Paton Welding Journal #10 (2020) 13-18. DOI: https://doi.org/10.37434/tpwj2020.10.03
[36] A. Kroma, M. Mendak, M. Jakubowicz, B. Gapiński, P. Popielarski, Non-Contact Multiscale Analysis of a DPP 3D-Printed Injection Die for Investment Casting, Materials 14/22 (2021) 6758. DOI: https://doi.org/10.3390/ma14226758
[37] A. Yadollahi, N. Shamsaei, S.M. Thompson, A. Elwany, L. Bian, Effects of building orientation and heat treatment on fatigue behavior of selective laser melted 17-4 PH stainless steel, International Journal of Fatigue 94/2 (2017) 218-235. DOI: https://doi.org/10.1016/j.ijfatigue.2016.03.014
[38] S. Beretta, M. Gargourimotlagh, S. Foletti, A. du Plessis, M. Riccio, Fatigue strength assessment of "as built" AlSi10Mg manufactured by SLM with different build orientations, International Journal of Fatigue 139 (2020) 105737. DOI: https://doi.org/10.1016/j.ijfatigue.2020.105737
[39] I.S. Raju, J.C. Jr. Newman, Stress-intensity factors for a wide range of semi-elliptical Surface cracks in finite-thickness plates, Engineering Fracture Mechanics 11/4 (1979) 817-829. DOI: https://doi.org/10.1016/0013-7944(79)90139-5
[40] X. Wu, In situ formation by laser cladding of a TiC composite coating with a gradient distribution, Surface and Coatings Technology 122/2-3 (2006) 111-115. DOI: https://doi.org/10.1016/S0257-8972(99)00045-6
[41] A. Stanula, W. Pilarczyk, Combined carbon content assessment method for powder metallurgy, Journal of Achievements in Materials and Manufacturing Engineering 114/1 (2022) 15-21. DOI: https://doi.org/10.5604/01.3001.0016.1479
[42] A. Majeed, A. Ahmed, A. Salam, M. Z. Sheikh, Surface quality improvement by parameters analysis, optimization and heat treatment of AlSi10Mg parts manufactured by SLM additive manufacturing, International Journal of Lightweight Materials and Manufacture 2/4 (2019) 288-295. DOI: https://doi.org/10.1016/j.ijlmm.2019.08.001
[43] M.-H. Hong, B.K. Min, T.-Y. Kwon, The Influence of Process Parameters on the Surface Roughness of a 3D-Printed Co–Cr Dental Alloy Produced via Selective Laser Melting, Applied Sciences 6/12 (2016) 401. DOI: https://doi.org/10.3390/app6120401
[44] L.A. Dobrzański, A.D. Dobrzańska-Danikiewicz, A. Achtelik-Franczak, L.B. Dobrzański, Comparative analysis of mechanical properties of scaffolds sintered from Ti and Ti6Al4V powders, Archives of Materials Science and Engineering 73/2 (2015) 69-81.